Facile Spray-Drying Assembly of Uniform Microencapsulates with Tunable Core–Shell Structures and Controlled Release Properties

Wenjie Liu,[†] Winston Duo Wu,[†] Cordelia Selomulya,*,[†] and Xiao Dong Chen[†,‡]

[†]Department of Chemical Engineering, Monash University, Clayton, Victoria 3800, Australia

[‡]Department of Chemical and Biochemical Engineering, College of Chemistry and Chemical Engineering, Xiamen University, 361005 Xiamen, Fujian Province, People's Republic of China

Ⓢ *Supporting Information*

ABSTRACT: Microencapsulates with defined core–shell structures are of interest for applications, such as controlled release and encapsulation, because of the feasibility of fine-tuning individual functionalities of different parts. Here, we report a new approach for efficient and scalable production of such particles. Eudragit RS (a co-polymer of ethyl acrylate, methyl methacrylate, and a low content of methacrylic acid ester with quaternary ammonium groups) was used as the main shell component, with silica as the core component, formed upon a single-step spray-drying assembly. The method is capable of forming uniform core–shell particles from homogeneous precursors without the use of any organic solvents. Evaporation-induced self-assembly attained the phase separation among different components during drying, resulting in the core–shell spatial configuration, while precise control over particle uniformity was accomplished via a microfluidic jet spray dryer. Direct control over shell thickness can be achieved from the ratio of the core and shell ingredients in the precursors. A fluorescent compound, rhodamine B, is used as a highly water-soluble model component to investigate the controlled release properties of these microencapsulates, with the release behaviors shown to be significantly dependent upon their architectures.
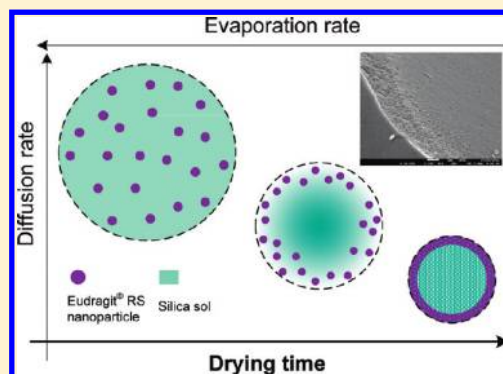
1. INTRODUCTION

Encapsulation of drugs or other active ingredients into small particulates has long been recognized as an effective way for their delivery.[1,2] Composite core–shell microparticles, usually with a structural core domain covered by a polymeric shell, have been widely adapted for encapsulation purposes, because of a better control of release kinetics of the incorporated active ingredients.[3–5] The core and shell domains could comprise various materials, with the size and structure adjusted to tailor the functionalities.[6–8] Other examples of the use of core–shell assemblies were included as templates to form hollow particles (by core removal)[9] or to use cheaper core materials as supports for more valuable shell components.[10,11] Various studies have been carried out to fabricate particulates with core–shell structures using approaches such as layer-by-layer absorption,[10] emulsion phase evaporation,[12] interfacial polymerization,[13] or coaxial electrospray.[1,14] The major drawbacks for these methods are the sophisticated apparatus, often batchwise operating steps, long reaction time, and use of organic solvents and often rigorous post-treatments to recover the final particles.[15,16] Significant proportions of the active therapeutic agents are commonly lost during the process because of the numerous steps involved.

Spray-drying technology, on the other hand, offers a simple and scalable means of particle production. However, most spray-dried particles generally display a solid dispersion state.[17,18] It has been postulated previously that some species, such as colloidal nanoparticles and large polymeric molecules, could precipitate prior to the other solute molecules to form a shell at the initial stage of spray drying,[19,20] because of their relatively small diffusivity from their large hydrodynamic size.[21] This phenomenon can be explained from the Stokes–Einstein equation: $D_s = k_B T/(6\pi\eta R_H)$, where D_s is the diffusion coefficient of the solute, k_B is Boltzman's constant, η is the viscosity of the solvent, T is the temperature, and R_H is the hydrodynamic radius of the solute.[22,23] Thus, there could be a relative enrichment of larger molecules on the surface of the spray-dried particles, which was demonstrated in our previous work,[18,24] although no distinctive internal structures were formed. To the best of our knowledge, no core–shell structure formation from a homogeneous precursor via spray drying using a single nozzle (orifice) has ever been reported.

In this study, we used a stable precursor containing hydrolyzed tetraethyl orthosilicate (referred to as TEOS) and Eudragit RS 30D (referred to as RS) in water (both of them are commonly used biocompatible pharmaceutical excipients). The hydrodynamic diameters (i.e., particle size in suspension as measured by dynamic light scattering) of hydrolyzed TEOS and RS were
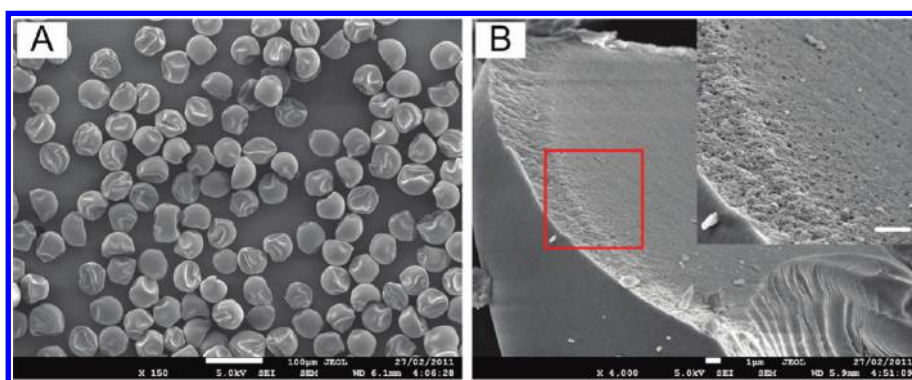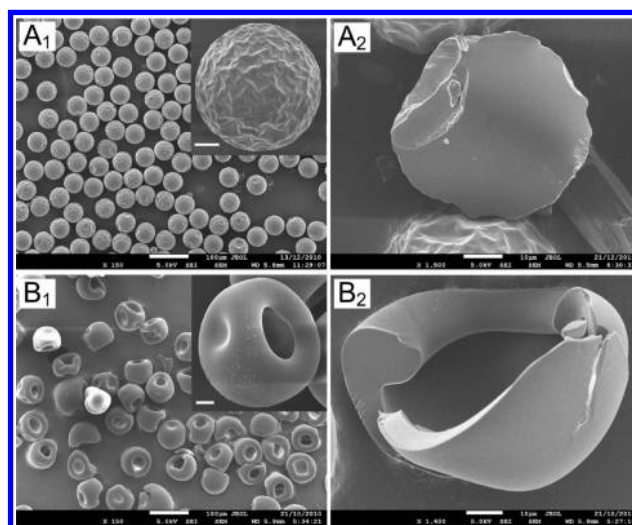
Table 1. Composition of the Precursors for Spray Drying

composition number	silica (%, w/v)	Eudragit RS (%, w/v)	particle size (μm)	rhodamine B loading (%)
$Si_{3.0}$	3.0		55.30 ± 1.94	97.37 ± 3.85
$Si_{2.5}RS_{0.5}$	2.5	0.5	55.04 ± 2.60	96.19 ± 3.44
$Si_{1.5}RS_{1.5}$	1.5	1.5	88.80 ± 5.42	94.24 ± 2.81
$Si_{1.0}RS_{2.0}$	1.0	2.0	98.91 ± 4.91	95.66 ± 3.83
$Si_{0.5}RS_{2.5}$	0.5	2.5	105.50 ± 5.51	95.45 ± 1.45
$RS_{3.0}$		3.0	76.10 ± 3.63	98.90 ± 2.39

Figure 1. FESEM images of the spray-dried microparticles of composition $Si_{2.5}RS_{0.5}$*: (A) particle overall view and (B) cross-section of a typical particle showing the core−shell structure (inset scale bar of 1 μm).
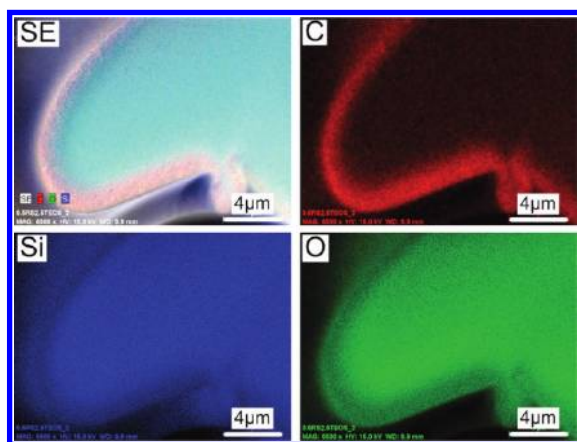
Figure 2. Elemental distribution maps for the cross-section of $Si_{2.5}RS_{0.5}$* microparticles (SE, overall distribution of elements carbon, silicon, and oxygen; C, distribution of element carbon; Si, distribution of element silicon; and O, distribution of element oxygen).

Figure 3. SEM images of spray-dried microparticles with rhodamine B: (A) $Si_{3.0}$ and (B) $RS_{3.0}$ (inset scale bar of 10 μm).

around 1 and 120 nm, respectively. The distinct hydrodynamic sizes, in relation to diffusivity, were expected to induce the precipitation of RS faster than hydrolyzed TEOS and should result in core−shell structures upon self-assembly during spray drying. We also employed rhodamine B as a model drug to evaluate the release behavior from these particles, particularly in relation to the shell thickness. It is also worth noting that the size of the delivery vehicles is an important parameter for their optimal performance,[25,26] while ordinary lab-scale spray dryers usually produce particles of various characteristics, e.g., size, morphology, and structure within the same batch.[27,28] The polydispersity of the particles might induce poorly controllable functionalities, while the lack of reproducibility renders it difficult

to correlate the properties of particles formed to those of the precursors and other process parameters. Here, to achieve uniformity of the particles, a specially designed microfluidic spray dryer was employed to produce monodisperse microparticles with high reproducibility and comparatively high yield of production of such particles (collection efficiency >70% with a typical production rate of several grams per hour).

2. EXPERIMENTAL SECTION

2.1. Materials. Eudragit RS 30D (a co-polymer of ethyl acrylate, methyl methacrylate, and a low content of methacrylic acid ester with
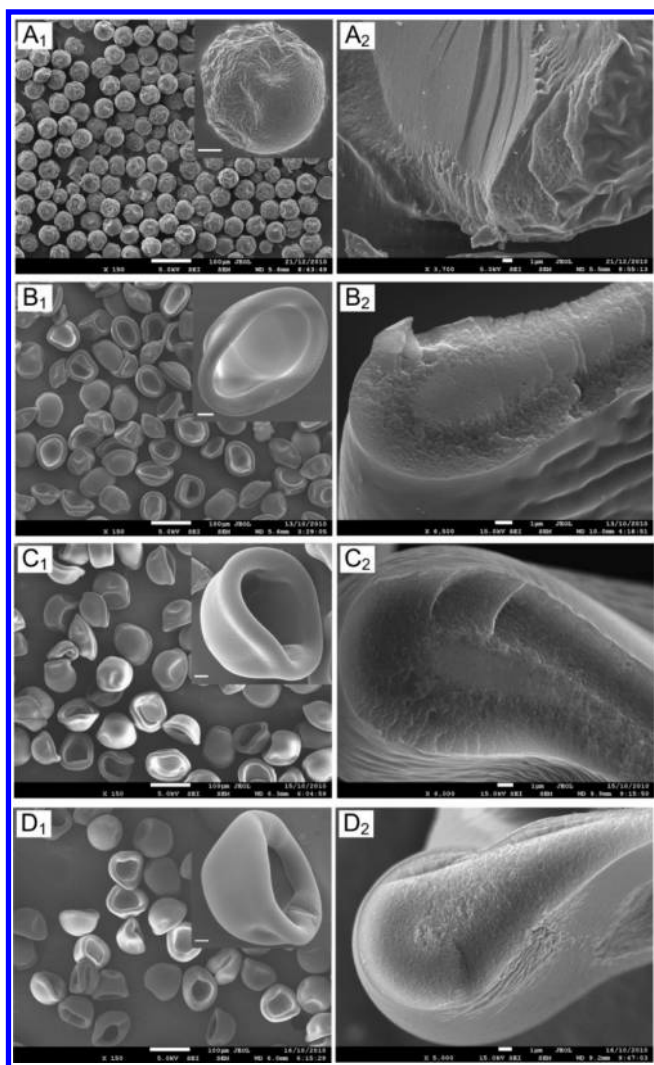
Figure 4. SEM images of spray-dried microparticles with rhodamine B: (A) $Si_{2.5}RS_{0.5}$, (B) $Si_{1.5}RS_{1.5}$, (C) $Si_{1.0}RS_{2.0}$, and (D) $Si_{0.5}RS_{2.5}$ (inset scale bar of 10 μm).

Figure 5. Schematic showing the evolution of a droplet containing both Eudragit RS and hydrolyzed TEOS during the drying process. Phase segregation of Eudragit RS and hydrolyzed TEOS because of different diffusion rates resulted in the silica core—Eudragit RS shell configuration for these composite particles.

silica sols and diluted Eudragit RS dispersions were freshly prepared with the same procedures for each experiment.

2.3. Microparticle Fabrication. Monodisperse droplets were generated from precursor solution by a microfluidic aerosol nozzle system, with an orifice diameter of 75 μm. Briefly, the precursor solutions were fed into a standard steel reservoir, and dehumidified instrument air was used to force the liquid in the reservoir to jet through the nozzle. The liquid jet was broken into droplets by disturbance from vibrating piezoceramics. The droplet formation mode was monitored by a digital SLR camera (Nikon, D90) with a speed light (Nikon SB-400) and a microlens (AF Micro-Nikkor 60 mm f/2.8D). The liquid flow rate and applied disturbance frequency were adjusted to best achieve monodisperse droplet formation.[29] These monodisperse droplets obtained were well-dispersed and dried with 146 and 83 °C as the inlet and outlet temperatures, respectively.

2.4. Particle Characterization. Images of microparticles were recorded by light microscopy (Motic B1-223A, U.K.). Particle size and size distribution were analyzed using the software package Motic Images Plus 2.0 ML and ImageJ. The average particle size ($\bar{d}$) was defined as $\bar{d} = \Sigma_{i=1}^{n}(d_i)/N$, and the standard deviation of the particle size was described as $SD = ((\Sigma(d_i - \bar{d})^2)/(N-1))^{1/2}$, where d_i was the diameter of the ith particle and N was the total number of particles counted. The morphology and structure of microparticles before and after the release test were characterized by a Stereo Zoom optical microscope (Olympus SZX-16, Japan) and field-emission scanning electron microscopy (FESEM, JEOL 7001F, Japan).

2.5. Controlled Release Test. In a typical experiment, the microparticles (25 mg) were weighted into a 100 mL conical flask and 50 mL of PBS release medium (pH 7.4) was transferred into the flask. The flask was kept in a shaking incubator at 37 °C with constant agitation (100 rpm). At certain time intervals, 1 mL of the release medium was withdrawn from the flask and replaced with the same amount of fresh release medium. Collected samples were transferred into 1.7 mL microtubes, centrifuged for 5 min at 10 000 rpm (Heal force, Neofuge 23R), and subjected to assay immediately. The content of rhodamine B in the sample was determined by a microplate reader (SpectraMax M2e, Molecular Devices) at the wavelength of maximum absorbance (555 nm). Each sample was performed in triplicate.

2.6. Encapsulation Efficiency. The total amount of rhodamine B encapsulated into microparticles was determined by dissolving an

quaternary ammonium groups, 30% aqueous dispersion) was kindly provided by Evonik Degussa Industries (Australia). The average particle size of the Eudragit RS dispersion was 120.2 ± 1.2 nm measured from 1% (w/v) Eudragit RS dispersion by the dynamic light scattering method (Malvern Zatasizer, Nano-ZS). TEOS, rhodamine B, and phosphate-buffered saline (PBS, pH 7.4, consisting of 0.138 M NaCl, 0.0027 M KCl, 0.01 M $Na_2HPO_4 \cdot 2H_2O$, and 0.001 76 M KH_2PO_4) were purchased from Sigma-Aldrich (Australia). Hydrochloric acid, absolute ethanol, and sodium hydroxide of analytical grade were from Ajax Finechem (Australia) and Merck (Australia), respectively. Deionized water (Milli-Q) was used for all precursor preparations.

2.2. Precursor Preparation. A total of 22.29 mL of TEOS was added to 20 mL of 0.1 N HCl solution with continuous stirring at room temperature. The acidic hydrolysis was performed for 30 min to obtain a homogeneous transparent sol. The sol was further diluted to 200 mL using deionized water to achieve a 3.0% (w/v) silica sol (calculated by the amount of silica dioxide obtained after the spray-drying process). Meanwhile, a dispersion of 3% (w/v) Eudragit RS was also prepared. For the precursors used in the preparation of composite particles, 3% silica sol and 3% Eudragit RS were mixed in certain ratios, followed by the addition of rhodamine B for 5 min (as indicated in Table 1). The as-prepared precursors were then spray-dried without further delay. The
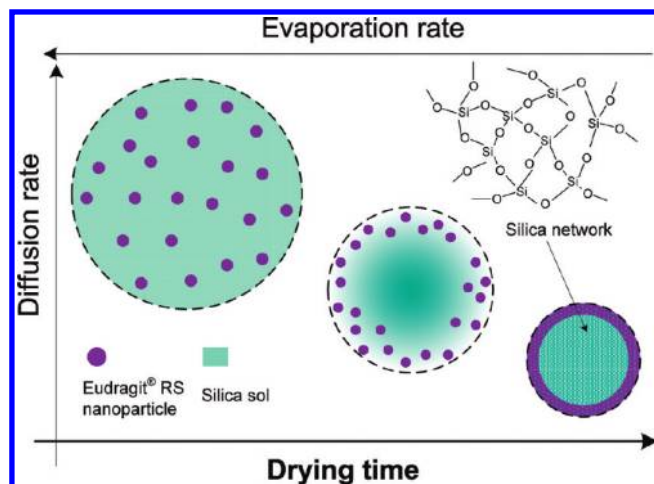
accurately weighed amount of microparticles in a 10 mL mixture of ethanol and NaOH solution. After the dissolution of particles, the solutions were centrifuged for 5 min at 10 000 rpm and the amount of rhodamine B in the supernatant was determined by the microplate reader under 555 nm. The loading efficiency of rhodamine B was calculated by dividing the amount of rhodamine B in the microparticles by the initial amount added.

3. RESULTS AND DISCUSSION

3.1. Particle Engineering and Structural Properties. The single-step assembly of uniform microparticles was accomplished
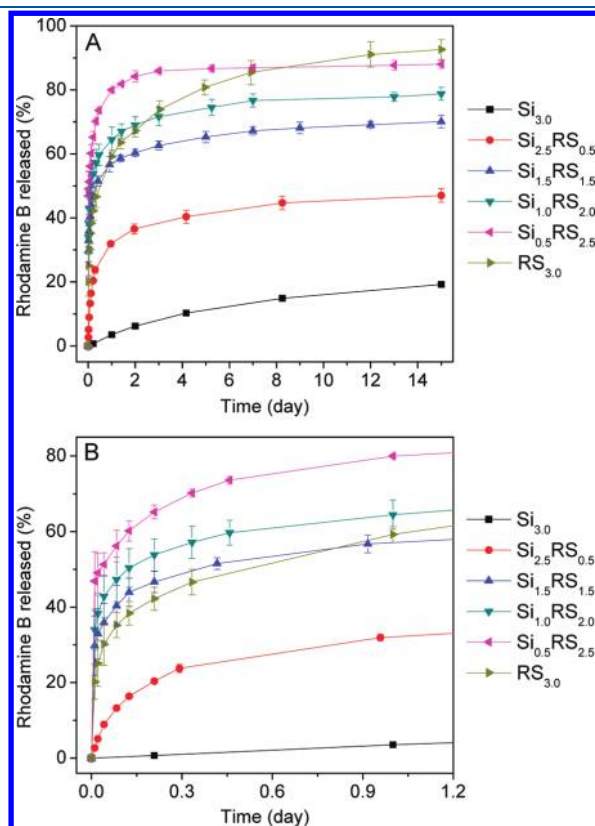

Figure 6. (A) Release profiles of rhodamine B from spray-dried microparticles and (B) inset of the release profile for the first 1.2 days.

via a microfluidic spray-drying technique,[30] with the precursor compositions listed in Table 1. Figure S1 of the Supporting Information showed the monodisperse droplets generated using the microfluidic spray-drying method. Microparticles with very narrow size distribution can be generated, with the control of the particle size depending upon the relative concentrations of the components in the precursors and the size of the initial droplets.[24,29] Figure 1A showed the FESEM image of uniform microparticles spray dried from a precursor containing 2.5 wt % hydrolyzed TEOS and 0.5 wt % RS only (referred to as $Si_{2.5}RS_{0.5}{}^{*}$).

The application of evaporation-induced self-assembly has given rise to the formation of various interesting mesoscopically ordered nanostrucures.[31,32] Here, a similar phenomenon was used to achieve phase separation between RS and hydrolyzed TEOS to form the core—shell structures in a single step, as confirmed by the FESEM image of the cross-sections of the particles (Figure 1B). To verify the morphology as well as their compositions, the particles were subjected to elemental distribution analysis. Figure 2 displayed a representative elemental distribution map of the cross-section of $Si_{2.5}RS_{0.5}{}^{*}$ microparticles exhibiting a distinct core—shell morphology. The elemental "C" originated from RS was mostly present on the outer layer of the particles, indicating the formation of a mostly polymeric shell, whereas the elementals "Si" and "O" were mostly concentrated on the inner particles, implying silica as the main component of the inner structure. Pure RS or silica microparticles were spray-dried for comparison, with silica particles showing a dense, almost spherical shape (Figure 3A), while the polymeric particles appeared more deformable (Figure 3B).

We could also control the internal configurations of the microparticles, as well as the shell thickness, by varying the ratio of these materials in the precursors. All particulate systems showed homogeneous properties in size and shape, while their morphology was strongly related to the initial precursor compositions, with the composite particles showing evolving morphologies in between those of pure silica and pure polymeric particles depending upon the ratio of each component in the composites (Figure 4). The corresponding size distributions for these microparticles from statistical analysis were shown in Figure S2 of the Supporting Information. Pure RS and pure silica microparticles exhibited uniform spatial configuration, as seen from their cross-sections (Figure 3). On the other hand, the composite
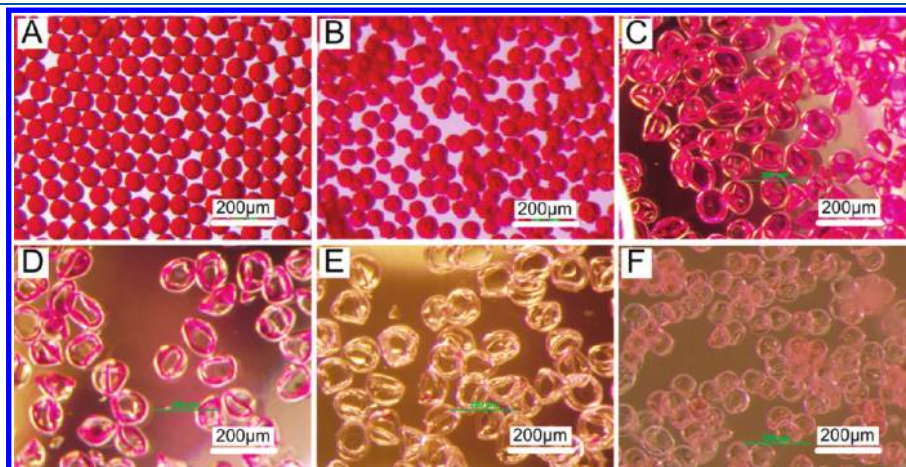

Figure 7. Optical images of microparticles after the release test: (A) $Si_{3.0}$, (B) $Si_{2.5}RS_{0.5}$, (C) $Si_{1.5}RS_{1.5}$, (D) $Si_{1.0}RS_{2.0}$, (E) $Si_{0.5}RS_{2.5}$, and (F) $RS_{3.0}$.

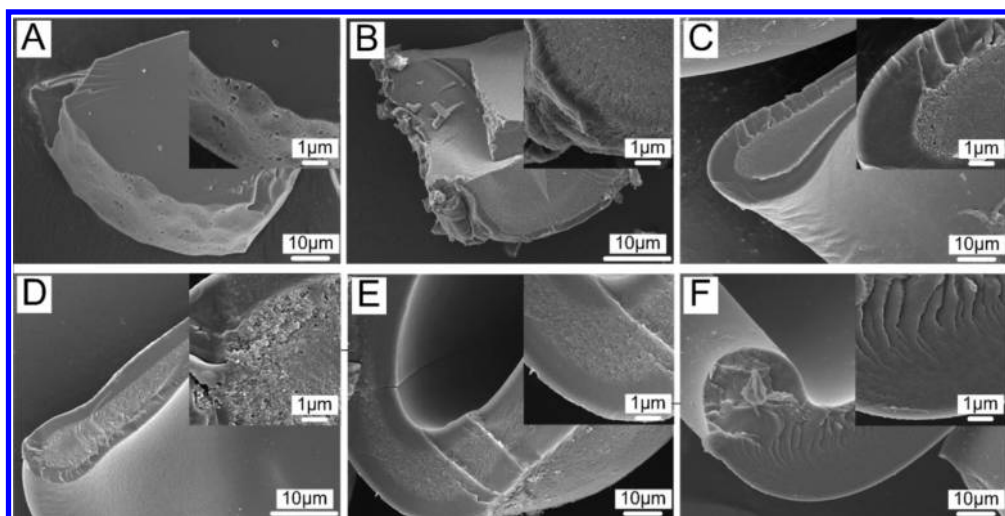**Figure 8.** FESEM images of microparticles after the release test: (A) $Si_{3.0}$, (B) $Si_{2.5}RS_{0.5}$, (C) $Si_{1.5}RS_{1.5}$, (D) $Si_{1.0}RS_{2.0}$, (E) $Si_{0.5}RS_{2.5}$, and (F) $RS_{3.0}$.

particles demonstrated core—shell features (Figure 4), with an increasing relative shell thickness with a decreasing silica/RS ratio. These outcomes suggested that the strategy could be used to directly control the core—shell properties from precursor compositions. Elemental distribution maps of the cross-sections confirmed the polymeric shell with silica core structures, as also shown in Figures S3—S7 of the Supporting Information.

A possible mechanism of forming the core—shell-structured microencapsulates is given here. The particle formation process during drying can be described by solvent evaporation and diffusion of solutes in the droplet because of the heat and mass transfers. Solvent evaporation causes surface recession of the droplet. The removal of solvent and the receding droplet surface lead to a diffusion flux of the solutes toward the center of the droplet.[21] Because a single type of the main solvent of deionized water was used in the system (with a negligible amount of ethanol generated during the TEOS hydrolysis process), the distribution mode of the solutes in the dried particles would be mainly determined by their respective diffusion rates during solvent evaporation. RS existing as colloidal nanoparticles in the initial droplet was of a much larger average hydrodynamic size than the hydrolyzed TEOS molecules, consequently precipitating earlier to form a shell. Although there was a small fraction of silica precipitating together with the RS in the shell, the majority of hydrolyzed TEOS was still diffusing inward, while all of the RS have already precipitated, resulting in the formation of a core completely composed of silica (Figure 5).

3.2. Controlled Release Properties. The loadings of rhodamine B as listed in Table 1 indicated that almost 100% of the compound was encapsulated into the microencapsulates using this assembly method. The loading efficiency was significantly higher than those attainable by wet chemistry-based approaches that are generally less than 50% encapsulation. The single-step particle formation process ensured that any added active ingredients could be loaded almost completely into the particles, while a practical (as well as scalable) yield could be obtained without any required post-separation/purification steps. The benefits of this technique are significant, particularly in handling expensive components, such as active therapeutic agents.

The release characteristics of the microencapsulates in phosphate buffer at pH 7.4 were shown in Figure 6A. Pure silica microparticles ($Si_{3.0}$) and pure RS microparticles ($RS_{3.0}$) displayed very distinctive release behaviors. $Si_{3.0}$ particles showed a slow release behavior with only 20% of the loaded rhodamine B released in a 15 day test period, while $RS_{3.0}$ particles released almost 100% within the same period. The composite particles demonstrated significantly different release kinetics compared to the single-component particles, with the total release rate increasing with an increasing RS amount (and thus the shell thickness). The release profiles can be generally divided into two parts: (1) a relatively faster initial release stage (or burst) because of water uptake and swelling of the RS polymer, leading to the release of rhodamine B from the shell, followed by (2) a more sustained release stage because of the dense silica core texture and longer diffusion route from the core.[33,34] The two-stage release characteristics of the composite particles represented a combination of the release kinetics from pure RS and pure silica microparticles, i.e., the relatively fast release of RS (the shell material) and the slow release of silica (the core component). Hence, when the internal configuration of the particles was manipulated directly from the composition of the precursors, the controlled release functionality can be tuned accordingly.

Interestingly, the initial release profiles (Figure 6B) indicated that pure RS particles ($RS_{3.0}$) had a slower initial release rate than some of the core—shell particles ($Si_{1.5}RS_{1.5}$, $Si_{1.0}RS_{2.0}$, and $Si_{0.5}RS_{2.5}$). A possible explanation for this phenomenon was the slightly more porous texture of the polymeric shell (Figure 4) compared to particles composed only of RS (Figure 3B), which could be due to the presence of some silica on the shell for these composites (as shown from the elemental distribution map on Figures S4—S7 of the Supporting Information). This type of structure would facilitate buffer penetration through the shell and, thus, accelerated the initial release rate of rhodamine B closer to the surface. However, rhodamine B encapsulated within the mainly silica core of these composites would still be slow to release, so that the overall percentage of rhodamine B released after 15 days was lower than that from pure RS particles.

The optical microscope and FESEM images of the microencapsulates after the release test (Figures 7 and 8) displayed decreasing residual rhodamine B remaining in the particles (as indicated by the red color) with an increasing RS ratio, consistent

with the observed release profiles. A transparent shell and red core structure were clearly observed in Figure 7D, confirming the almost complete release from the shell and the incomplete release from the core. There was no noticeable difference in the particle shape after the release test (Figure S8 of the Supporting Information). However, FESEM images of the particle cross-section (Figure 8) indicated the different extents of erosion for the silica core. Because RS was insoluble in aqueous medium, no significant change was observed for $RS_{3.0}$ particles after the release test. Pure silica particles only showed minor surface erosion, while the inner particle was still very dense, indicating that liquid penetrating through the pure silica matrix was negligible, with only rhodamine B located on or near the surface released. However, the composite particles displayed noticeably eroded features of the core after release tests, possibly because more buffer was able to go through the slightly porous polymeric shell, eroding the core.

4. CONCLUSION

A novel route for fast, scalable, and continuous assembly of highly monodispersed core—shell microencapsulates was presented here. Because the core—shell architecture could be formed directly by evaporation-induced self-assembly during the single-step spray-drying process, no prolonged chemical reactions or organic solvents were needed. The shell thickness can be easily tuned by adjusting the ratio of the materials in the precursors. The resultant microencapsulates were shown to encapsulate almost 100% of the active component (in this case, a water-soluble compound, rhodamine B), while the release rates could be directly correlated to the microstructures. This study provides a new scope for practical synthesis of hybrid nanocomposites and functional heterostructures, including core—shell structures with distinct controlled release properties for each section.

■ ASSOCIATED CONTENT

ⓢ Supporting Information.   Extended details of the experiments and auxiliary results related to the present study. This material is available free of charge via the Internet at http://pubs.acs.org.

■ AUTHOR INFORMATION

Corresponding Author
*Telephone: +61-3-99053436. Fax: +61-3-99055686. E-mail: cordelia.selomulya@monash.edu.

■ ACKNOWLEDGMENT

■ REFERENCES

(1) Choi, D. H.; Park, C. H.; Kim, I. H.; Chun, H. J.; Park, K.; Han, D. K. *J. Controlled Release* **2010**, *147*, 193–201.

(2) Pancholi, K.; Stride, E.; Edirisinghe, M. *Langmuir* **2009**, *25*, 10007–10013.

(3) Ito, R.; Boris, G.; Shinohara, K. *Chem. Eng. Sci.* **2005**, *60*, 5415–5424.

(4) Fakhrullin, R. F.; Minullina, R. T. *Langmuir* **2009**, *25*, 6617–6621.

(5) Lee, W. L.; Hong, M.; Widjaja, E.; Loo, S. C. J. *Macromol. Rapid Commun.* **2010**, *31*, 1193–1200.

(6) Lee, W. L.; Loei, C.; Widjaja, E.; Loo, S. C. J. *J. Controlled Release* **2011**, *151*, 229–238.

(7) Berkland, C.; Pollauf, E.; Pack, D. W.; Kim, K. *J. Controlled Release* **2004**, *96*, 101–111.

(8) Jo, C.; Lee, H. J.; Oh, M. *Adv. Mater.* **2011**, *23*, 1716–1719.

(9) Akamatsu, K.; Chen, W.; Suzuki, Y.; Ito, T.; Nakao, A.; Sugawara, T.; Kikuchi, R.; Nakao, S.-i. *Langmuir* **2010**, *26*, 14854–14860.

(10) Shenoy, D. B.; Antipov, A. A.; Sukhorukov, G. B.; Möhwald, H. *Biomacromolecules* **2003**, *4*, 265–272.

(11) Lin, C.; Li, Y.; Yu, M.; Yang, P.; Lin, J. *Adv. Funct. Mater.* **2007**, *17*, 1459–1465.

(12) Lee, W. L.; Foo, W. L.; Widjaja, E.; Loo, S. C. J. *Acta Biomater.* **2010**, *6*, 1342–1352.

(13) Dziomkina, N. V.; Hempenius, M. A.; Vancso, G. J. *Eur. Polym. J.* **2006**, *42*, 81–91.

(14) Lee, Y.-H.; Mei, F.; Bai, M.-Y.; Zhao, S.; Chen, D.-R. *J. Controlled Release* **2010**, *145*, 58–65.

(15) Nie, Z.; Xu, S.; Seo, M.; Lewis, P. C.; Kumacheva, E. *J. Am. Chem. Soc.* **2005**, *127*, 8058–8063.

(16) De Geest, B. G.; De Koker, S.; Gonnissen, Y.; De Cock, L. J.; Grooten, J.; Remon, J. P.; Vervaet, C. *Soft Matter* **2010**, *6*, 305–310.

(17) Janssens, S.; Anné, M.; Rombaut, P.; Van den Mooter, G. *Eur. J. Pharm. Sci.* **2009**, *37*, 241–248.

(18) Wu, W. D.; Liu, W.; Selomulya, C.; Chen, X. D. *Soft Matter* **2011**, DOI: 10.1039/C1SM05879G.

(19) Sen, D.; Mazumder, S.; Melo, J. S.; Khan, A.; Bhattyacharya, S.; D'Souza, S. F. *Langmuir* **2009**, *25*, 6690–6695.

(20) Sen, D.; Melo, J.; Bahadur, J.; Mazumder, S.; Bhattacharya, S.; Ghosh, G.; Dutta, D.; D'Souza, S. *Eur. Phys. J. E: Soft Matter Biol. Phys.* **2010**, *31*, 393–402.

(21) Vehring, R.; Foss, W. R.; Lechuga-Ballesteros, D. *J. Aerosol Sci.* **2007**, *38*, 728–746.

(22) Tsapis, N.; Bennett, D.; Jackson, B.; Weitz, D. A.; Edwards, D. A. *Proc. Natl. Acad. Sci. U.S.A.* **2002**, *99*, 12001–12005.

(23) Rizi, K.; Green, R. J.; Donaldson, M.; Williams, A. C. *J. Pharm. Sci.* **2011**, *100*, 566–579.

(24) Liu, W.; Wu, W. D.; Selomulya, C.; Chen, X. D. *Int. J. Chem. Eng* **2011** No. 267218.

(25) Tran, V.-T.; Benoît, J.-P.; Venier-Julienne, M.-C. *Int. J. Pharm.* **2011**, *407*, 1–11.

(26) Wang, J.-T.; Wang, J.; Han, J.-J. *Small* **2011**, *7*, 1728–1754.

(27) Sen, D.; Melo, J. S.; Bahadur, J.; Mazumder, S.; Bhattacharya, S.; D'Souza, S. F.; Frielinghaus, H.; Goerigk, G.; Loidl, R. *Soft Matter* **2011**, *7*, 5423–5429.

(28) Mezzenga, R.; Ulrich, S. *Langmuir* **2010**, *26*, 16658–16661.

(29) Wu, W. D.; Lin, S. X.; Chen, X. D. *AIChE J.* **2011**, *57*, 1386–1392.

(30) Wu, W. D.; Amelia, R.; Hao, N.; Selomulya, C.; Zhao, D.; Chiu, Y.-L.; Chen, X. D. *AIChE J.* **2011**, DOI: 10.1002/aic.12489.

(31) Lu, Y.; Fan, H.; Doke, N.; Loy, D. A.; Assink, R. A.; LaVan, D. A.; Brinker, C. J. *J. Am. Chem. Soc.* **2000**, *122*, 5258–5261.

(32) Lu, Y.; Fan, H.; Stump, A.; Ward, T. L.; Rieker, T.; Brinker, C. J. *Nature* **1999**, *398*, 223–226.

(33) Liu, W.; Wu, W.; Selomulya, C.; Chen, X. D. *Soft Matter* **2011**, *7*, 3323–3330.

(34) Kristmundsdottir, T.; Gudmundsson, O. S.; Ingvarsdottir, K. *Int. J. Pharm.* **1996**, *137*, 159–165.